Numerical simulation of the sea water optical and microphysics characteristics in the problems of lidar sensing

V.V. Veretennikov

Institute of Atmospheric Optics,
Siberian Branch of the Russian Academy of Sciences, Tomsk

Received December 25, 2000

The results of numerical modeling of light scattering characteristics of polydisperse suspension in seawater in the small-angle approximation are presented. The suspension is formed from particles of two fractions: fine particles of terrigenic origin and the coarse ones of biogenic origin. Variations of their parameters and ratios between the fractions were taken into account. The results obtained by modeling are necessary as *a priori* information in solving inverse problems of laser sensing of seawater.

Introduction

When sensing seawater with a lidar, the lidar return depends on multiple scattering of light, which can be taken into account in the small-angle approximation.[1,2] To make use of this approximation, one usually chooses the extended small-angle part of the scattering phase function. Such a small-angle scattering phase function is often approximated by means of elementary functions of the type of exponent[3] or a gaussoid.[4] The approximate formula for describing, in the range of small angles, light scattering by particles whose refractive index is close to 1 was proposed in Ref. 5. This formula was obtained from the general Mie formulas and, in contrast from Refs. 3 and 4, it describes the dependence of the scattering phase function on the particle size in an explicit form.

Efficiency of solving the problems of laser sounding of sea, as well as other inverse problems, significantly depends on how correctly the *a priori* information about the medium under study is being taken into account. The fraction of the single scattered energy in the range of small angles is one of the *a priori* selected parameters in the problem under consideration. This value is determined by the ratio of the small-angle scattering coefficient σ_1 to its true value $a_1 = \sigma_1/\sigma$ and can be defined as the small-angle asymmetry factor. The *a priori* data on the small-angle scattering phase function is necessary for reconstruction of the profile of extinction coefficient from lidar signals taking into account the multiple scattering effect.[6,7] One can replace these data by the value of a single parameter, namely by the effective particle size in the case when the field-of-view angle of the receiver is sufficiently large. The purpose of this paper is to study numerically the effect of microstructure parameters of seawater suspension on their optical characteristics set *a priori* in inverting the data of lidar measurements.

1. Model of the scattering characteristics of sea water

The relative refractive index m of particles suspended in sea water is close to 1. This leads to the fact that the beams passing though the particle weakly deviate from the initial direction, and in the case when the phase shift of the wave $\delta = 2kr|m - 1| \approx 1$ after passing the particle is small, the interference of the diffracted and transmitted light occurs. As a result, one can describe the angular distribution of the radiation scattered by "soft" particles by means of the following approximate formula:

$$\beta_1(\gamma) = q\,\beta^{(D)}(\gamma), \qquad (1)$$

where $\beta^{(D)}(\gamma)$ is the coefficient of directed scattering in the Fraunhofer diffraction approximation that is determined by the known Airy formula[8]:

$$\beta^{(D)}(\gamma) = \frac{r^2 J_1^2(kr\gamma)}{\gamma^2}, \quad \gamma = \sin(\theta), \qquad (2)$$

θ is the scattering angle. The correction factor q in formula (1) has the form

$$q = 4|R(i\delta)|^2, \qquad (3)$$

where

$$R(z) = \frac{1}{2} + \frac{e^{-z}}{z} + \frac{e^{-z} - 1}{z^2} \qquad (4)$$

is the Hulst function.[9] Taking into account the form of $R(z)$ set by Eq. (4) one can obtain the formula for the function $q(\delta)$:

$$q(\delta) = 1 + \frac{4}{\delta^2}\left[1 + \left(1 + \frac{2}{\delta^2}\right)(1 - \cos\delta - \delta\sin\delta)\right]. \qquad (5)$$

The relation of the extinction efficiency factor $K_{ex} = \varepsilon/\pi r^2$ with the function $R(i\delta)$ follows from the optical theorem:

0235-6880/01/02 146-07 $02.00

$$K_{ex} = 4\mathrm{Re}[R(i\delta)], \quad (6)$$

from which one can obtain the Hulst formula for large "soft" particles

$$K_{ex} = 2 - \frac{4}{\delta}\sin\delta + \frac{4}{\delta^2}(1 - \cos\delta). \quad (7)$$

At $\delta > 3.5 - 4.0$ one can neglect the imaginary part $R(i\delta)$ as compared with the real one, $\mathrm{Im}\,[R(i\delta)] \ll \mathrm{Re}\,[R(i\delta)]$, that results in that

$$q = K_{ex}^2/4 = K_{sc}. \quad (8)$$

At $\delta \to \infty$, $K_{ex} \to 2$ the small-angle scattering efficiency factor $K_{sc} \to 1$ and $\beta_1(\gamma) = \beta^{(D)}(\gamma)$.

The correction coefficient q in the considered approximation does not depend on the scattering angle. So one can write for the normalized scattering phase function

$$x_1(\gamma) = \beta_1(\gamma)/\sigma_1 = x^{(D)}(\gamma),$$
$$x^{(D)}(\gamma) = \frac{J_1^2(kr\gamma)}{\pi\gamma^2}, \quad \sigma_1 = q\sigma^{(D)}, \quad (9)$$

from which it follows that the scattering phase function of "soft" particles of the same size has the same shape as in the case of diffraction on an opaque screen.

The normalized scattering phase function of a polydisperse ensemble of particles is determined by the formula

$$x_1(\gamma) = \int_{r_{min}}^{r_{max}} x^{(D)}(\gamma, r)\,\tilde{f}(r)\,dr, \quad (10)$$

where the function

$$\tilde{f}(r) = s(r)\,q(r) \Big/ \int_{r_{min}}^{r_{max}} s(r)\,q(r)\,dr \quad (11)$$

is proportional to the distribution of the geometric cross section of particles $s(r) = \pi r^2 n(r)$ in a unit volume with the weighting coefficient $q(r) = K_{sc}(r)$.

Analytical description of the lidar return[1,7] taking into account multiple scattering contains the dependence not on the small-angle scattering phase function itself, but on its Hankel transformation. The Hankel transformation $\tilde{x}^{(D)}(p)$ of the scattering phase function $x^{(D)}(\gamma, r)$ in the diffraction approximation (9) for particles of the same radius R has the form $\tilde{x}^{(D)}(p) = G(p/2kR)$, where the function $G(t)$ is determined by the formula

$$G(t) = \begin{cases} (2/\pi)\,[\arccos t - t\sqrt{1 - t^2}], & t \le 1, \\ 0, & t > 1. \end{cases} \quad (12)$$

Hence, for a polydisperse ensemble of particles we have

$$\tilde{x}_1(p) = \int_{r_{min}}^{r_{max}} G(p/2kr)\,\tilde{f}(r)\,dr. \quad (13)$$

As it was shown in Ref. 7, one can replace the function $\tilde{x}_1(p)$ in the lidar equation by the value of the derivative $\tilde{x}_1'(0)$ at zero point. Taking into account the formula for the derivative,

$$\frac{dG(t)}{dt} = -\frac{4}{\pi}(1 - t^2)^{1/2}, \quad t \le 1,$$

and differentiating $\tilde{x}_1(p)$ we obtain

$$\tilde{x}_1'(0) = -\frac{2}{\pi k}\int_{r_{min}}^{r_{max}} r^{-1}\,\tilde{f}(r)\,dr. \quad (14)$$

In the special case of a monodisperse medium, composed of particles with the radius R, the formula for the derivative $\tilde{x}_1'(0)$ becomes essentially simpler

$$\tilde{x}_1'(0) = -2/(\pi kR). \quad (15)$$

The integral in the right-hand side of formula (14) determines some effective particle size

$$R_{eff} = \left[\int_{r_{min}}^{r_{max}} r^{-1}\tilde{f}(r)\,dr\right]^{-1}. \quad (16)$$

Taking into account the introduced notation, formula (14) becomes analogous to formula (15) after substitution of R_{eff} instead of R. Thus, setting the derivative $\tilde{x}_1'(0)$ is equivalent to setting the effective particle radius R_{eff} (16).

Comparison of the results calculated using the small-angle scattering phase function by formula (1) with the data obtained from calculations by the precise Mie formulas for particles with the relative refractive indices 1.02 and 1.15 shows that formula (1) provides for obtaining the values of the coefficient of directed scattering by "soft" particles of practically any size with quite high accuracy.[5] The increase of the error in the case of applying the formula (1) occurs in approaching to the first zero of the Bessel function $J_1(\omega)$ that determines the position of the diffraction minimum at the point $\omega = kr\gamma \approx 3.83$. The positions of the diffraction minima for a polydisperse ensembles of particles are different for particles of different size, that leads to smoothing the scattering pattern. For this reason, the differences between calculations of the scattering phase function by precise and approximate formulas becomes less noticeable. As the model calculation show,[5] the error of the approximation is no more than 15% at the scattering angles $\theta \le 10°$ for the ensembles of particles with the power-law particle size distribution function (Junge distribution) $n(r) \sim r^{-\nu}$, $\nu = 5$ and the boundary size $kr_{min} = 20$, $kr_{max} = 200$.

2. Results of the numerical modeling

According to modern ideas about the microphysical properties of seawater, particles of two fractions, the

fine fraction of microdisperse particles of mineral (terrigenic) origin with the size $r < 1 - 2$ μm (relative refractive index 1.15) and the coarse fraction of particles of organic (biogenic) origin ($r > 1$ μm) with relative refractive index 1.02–1.05, suspended in water, make the principal contribution to the light scattering. The ratio of contributions of both fractions to the total scattering coefficient varies within wide limits. For example, according to data from Ref. 10, the contribution of organic particles of coarse fraction to the scattering coefficient is 22 to 78% depending on the type of water, that should naturally affect the shape of the scattering phase function of seawater and the behavior of lidar return signals.

When modeling the optical properties of the suspension, the size spectrum of fine terrigenic (t) particles was described by the power law

$$s_t(r) = A_t\, r^{-\nu} \qquad (17)$$

with the index $\nu = 1 - 4$ in the size range $0.2 \le r \le 2.0$ μm. The modified gamma–distribution

$$s_b(r) = A_b \left(\frac{r}{r_m}\right)^{\alpha} \exp\left\{-\frac{\alpha}{\gamma}\left[\left(\frac{r}{r_m}\right)^{\alpha} - 1\right]\right\} \qquad (18)$$

with the modal radius $r_m = 5 - 20$ μm and the fixed parameters $\alpha = 8$ and $\gamma = 3$ was chosen for description of the size spectrum of coarse fraction of biogenic (b) particles. The weighting factors A_t and A_b in the distribution $s_t(r)$ and $s_b(r)$ were selected so that it provided a prescribed ratio $\xi = \sigma_b/\sigma_t$ of the contributions coming from the fractions to the total scattering coefficient $\sigma = \sigma_t + \sigma_b$.

It was assumed in the investigations that the small-angle pattern of scattering is formed by all particles of b–fraction. As to the t–fraction, special attention was paid to the study of the effect of the "cutoff" boundary r_{min} of the smallest particles on the small-angle characteristics of scattering.

The ratio $a_1 = \sigma_1/\sigma$ and the effective particle size R_{eff} (16) are shown in Fig. 1 as functions of r_{min} at different contribution $p = \sigma_t/\sigma$ of t–fraction to the total scattering coefficient. The microstructure parameters of the fractions (17) and (18) were taken to be as follows: $\nu = 2$ and $r_m = 10$ μm. The extreme left position on the ordinate axis at $r_{min} = 0.2$ μm corresponds to the account of all particles of t–fraction of all size in the small-angle scattering according to the model (17). In this case at any value of p the ratio $a_1 > a_1^{(D)} = 0.5$, where $a_1^{(D)}$ is the portion of the diffracted light at scattering on optically "hard" large particles. From Fig. 1*a* follows an unexpected, in the first appearance, result which shows that as p increases, i.e., the role of t–fraction increases, the relative portion of energy scattered within the small-angle range also increases. This is explained by the peculiarities of the behavior of the factors K_{sc} and K_{ex} (7) leading to the increase of the ratio K_{sc}/K_{ex} at small r.

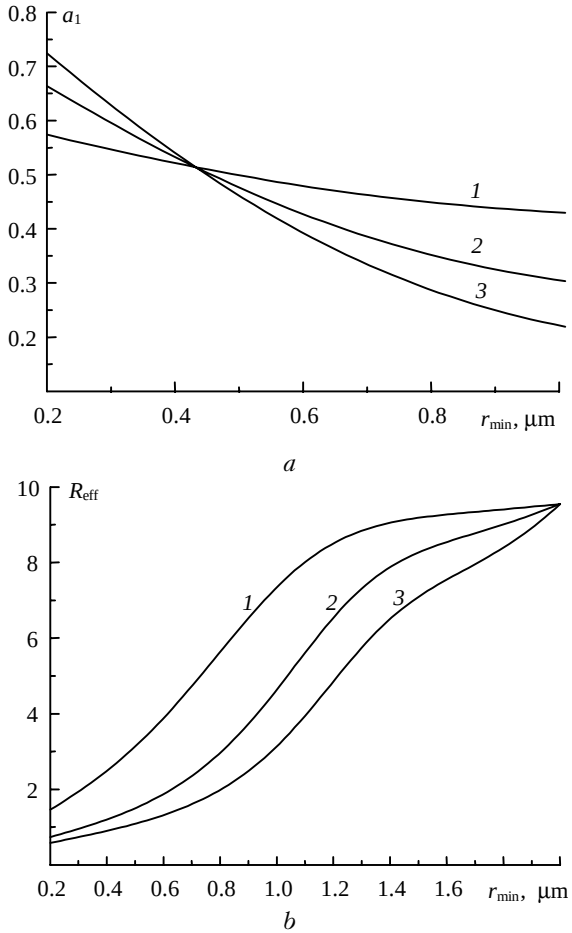

Fig. 1. The ratio $a_1 = \sigma_1/\sigma$ (*a*) and the effective radius R_{eff} (*b*) as functions of r_{min} for the polydisperse suspension of particles in water with the parameters of the microstructure $\nu = 2$ and $r_m = 10$ μm at $p = 0.2$ (*1*), 0.5 (*2*), and 0.7 (*3*).

The dependences of the parameter a_1 as function of r_{min} monotonically decrease, that is explained by removing the contribution of t–fraction $s_t(r)$ (17) at the particle radius from 0.2 μm to r_{min} from consideration in the small-angle scattering approximation. Naturally, the rate of the noted decrease is higher, as the role of t–fraction increases. This fact is interesting for practical applications to the problems of sounding, that all curves in Fig. 1*a* cross in the vicinity of the point $r_{min} = 0.45$ μm. Hence, taking into account the contribution only of the particles the radius of which exceed 0.45 μm to the small-angle scattering allows one to assume the parameter a_1 to be constant and to be equal to 0.52 at any ratio of t– and b–fractions in the range of the considered values of the parameter $p = 0.2 - 0.7$.

Let us consider now the behavior of the effective radius R_{eff} (16) shown in Fig. 1*b*. Let us preliminarily note that each of the fractions has its own effective radius of particles $R_{eff,\,t} = 0.46$ μm for $s_t(r)$ (17) at $r_{min} = 0.2$ μm and $R_{eff,\,b} \approx r_m = 10$ μm for $s_b(r)$ (18). The effective radius of the sum of fractions varies between these extreme values depending on the value of

the parameter p and r_{min}. It follows from the data shown in Fig. 1*b* that even a small addition of fine particles of t–fraction to large particles of b–fraction significantly decreases the value of the effective radius of the total suspension (p = 0.2, curve *1*).

The dependences analogous to those shown in Fig. 1 are presented in Fig. 2 for the case of the parameter ν in the distribution $s_t(r)$ increased up to 4.

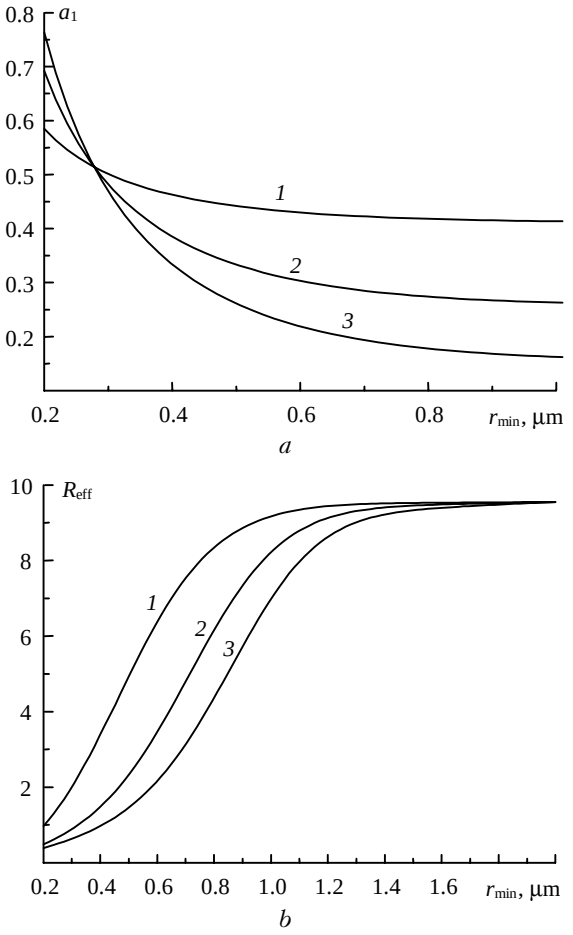

Fig. 2. The ratio a_1 (*a*) and the effective radius R_{eff} (*b*) as functions of r_{min} for the polydisperse suspension of particles in water with the microstructure parameters ν = 4 and r_m = 10 μm at p = 0.2 (*1*), 0.5 (*2*), and 0.7 (*3*).

Such a change leads to an increase in the degree to which the t–fraction is finely dispersed due to the enhanced role of the most small particles in it. The regularities noted for the dependences shown in Fig. 1 keep. Changes are related to movement of the cross point of the curves shown in Fig. 2*a* to the left to r_{min} = 0.3 μm. It is noticeable that the value of the parameter a_1 at this point is practically the same and is equal to 0.52.

As is seen from the comparison of Fig. 1*b* and Fig. 2*b*, as the parameter ν increases, the effective radius R_{eff}, as a function of r_{min}, increases more quickly and more quickly reaches "saturation". In this case the general decrease of the values R_{eff} is observed at ν = 4 at the left edge of the interval due to the decrease of the value R_{eff} of t–fraction down to 0.31 μm.

One more fact attracting attention when considering Figs. 1 and 2 is that the position of the point r_{min}, at which the parameter a_1 does not depend on the ratio of fractions in the mixture, is close to the value of the effective radius of particles of t–fraction (0.45 and 0.46 μm at ν = 2; 0.3 and 0.31 at ν = 4).

Principal conclusions drawn from the analysis of the data shown in Figs. 1 and 2 are also correct at variation of the parameters of the fraction of coarse organic particles $s_b(r)$ (18). The behavior of the parameter a_1 and the effective radius R_{eff} (16) for the modal radius of b–fraction r_m = 15 μm at different ratios of the fractions determined by the value p are shown in Fig. 3 as an example. The values of other parameters are the same as in Fig. 1. The position of the curves cross point in Fig. 3*a* practically has not changed. The difference observed in Fig. 3*b* is in widening the range of variation of the effective radius R_{eff} resulting from the increase of r_m.

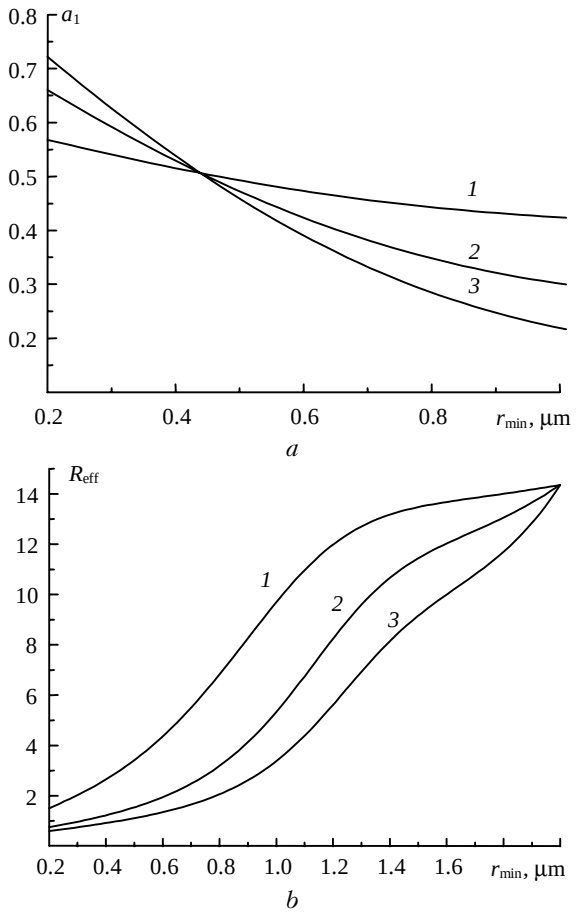

Fig. 3. The ratio a_1 (*a*) and the effective radius R_{eff} (*b*) as functions of r_{min} for the polydisperse suspension of particles in water with the parameters of the microstructure ν = 2 and r_m = 15 μm at p = 0.2 (*1*), 0.5 (*2*), and 0.7 (*3*).

The same characteristics a_1 and R_{eff} are shown in Fig. 4 at the invariant t–fraction (ν = 2) and equal

contribution of both fractions ($p = 0.5$) for the set of the values of modal radius r_m = 10, 15, and 20 μm. As is seen from Fig. 4, variations of the modal radius r_m practically do not affect the value of the a_1 ratio.

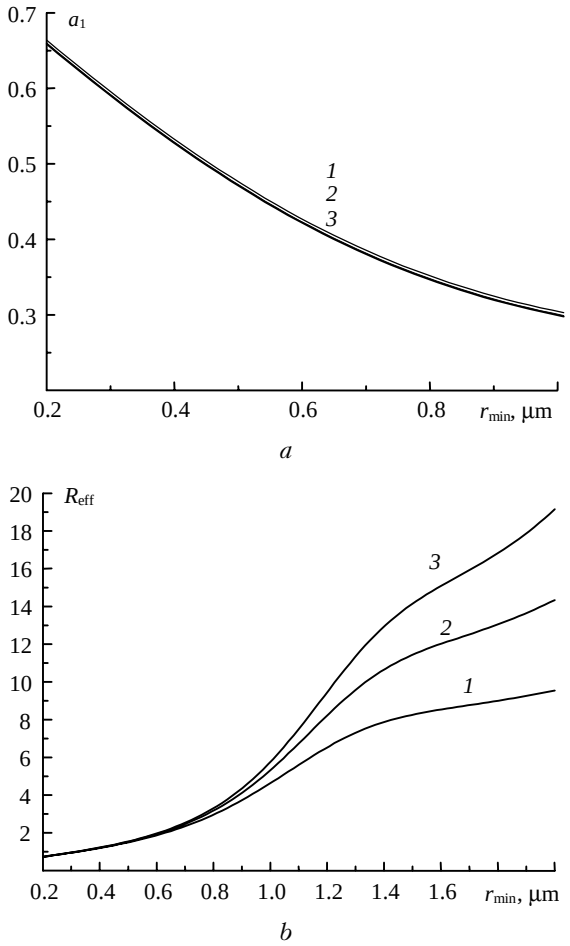

Fig. 4. The ratio a_1 (*a*) and the effective radius R_{eff} (*b*) as functions of r_{min} for the polydisperse suspension of particles in water with the microstructure parameters $\nu = 2$ and $p = 0.5$ for different modal radius of the particles of biogenic fraction r_m = 10 (*1*), 15 (*2*), and 20 μm (*3*).

One can draw the same conclusion on the behavior of the effective radius R_{eff} in the range of values r_{min}, where the effect of t–fraction is not weakened due to excluding the contribution of particles of the size less than 0.8–1 μm to the small-angle scattering pattern.

Let us next consider the behavior of small-angle scattering phase functions and their Hankel transformations. The modal radius of b–fraction was the same for all examples presented below and was equal to 15 μm.

The set of dependences is shown in Fig. 5 of the coefficient of directed light scattering $\beta_1(\theta)$ calculated for the considered microstructure model of the suspension with the parameters $\nu = 2$ and r_m = 15 μm and different lower boundary r_{min} of the particles of t–fraction taken into account in the formation of small-angle scattering pattern. The contributions of both fractions to the total scattering coefficient are assumed to be equal ($p = 0.5$). Curve *1* in Fig. 5 corresponds the account of all particles of t–fraction $s_t(r)$ (17) in the size range $0.2 \le r \le 2.0$ μm, and curve *5* is obtained at the total absence of these particles and is determined only by scattering on particles of b–fraction $s_b(r)$ (18). Other curves describe intermediate cases.

Two areas are distinguished in the curves (Fig. 5) in which scattering by one of the fractions is prevails. The boundary between these areas is in the scattering angle range θ = 1–2°. Position of the boundary moves inversely proportional to the change of the modal radius r_m of b–fraction. The function $\beta_1(\theta)$ in the limits of the first narrow area decreases by more than one order of magnitude, then its decrease becomes essentially slower, but nevertheless the total range of variations in the scattering angle range $\theta < 45°$ reaches 5–6 orders of magnitude. In the first area t–fraction makes insignificant contribution, and its variations here are weak. The second area is formed primarily due to the particles of t–fraction, and the changes in the microstructure of these particles well manifest themselves in transformation of the angular behavior of $\beta_1(\theta)$. As small particles are removed from consideration in the small-angle scattering phase function, it becomes more elongated. Local extrema appear in the curves $\beta_1(\theta)$ caused by narrowing the size range of t–fraction particles. For example, the equivalent radius of particles $r = 3.83/(k \sin\theta) \approx$ ≈ 0.69 μm corresponds to the minimum in the curve *3* (r_{min} = 0.6 μm), analogously, we have $r \approx 0.93$ μm for the minimum of curve *4* (r_{min} = 0.8 μm) at $\theta \approx 15.2°$.

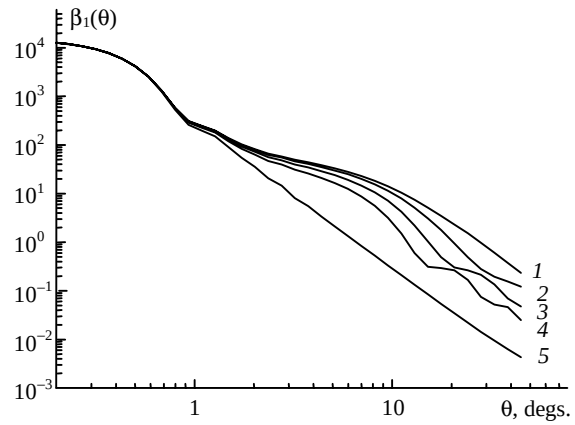

Fig. 5. The small-angle directed light scattering coefficient $\beta_1(\theta)$ for the polydisperse suspension of particles in water with the parameters of the microstructure $\nu = 2$, r_m = 15 μm, $p = 0.5$ and r_{min} = 0.2 (*1*), 0.4 (*2*), 0.6 (*3*), 0.8 (*4*), and 2.0 μm (*5*).

Figure 6 gives an idea of the ratio of the scattering phase functions of t–fraction (curve *1*) and b–fraction (curve *2*) in one of the total dependences $\beta_1(\theta)$ shown in Fig. 5 (curve *3*).

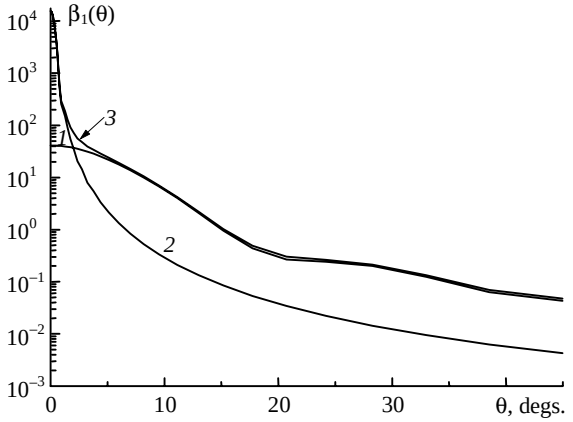

Fig. 6. Components of the coefficient of directed light scattering $\beta_1(\theta)$ for the particles of mineral fraction (*1*) with the parameters $\nu = 2$, $r_{min} = 0.6$ μm and biogenic fractions (*2*) with the modal radius $r_m = 15$ μm and their sum (*3*) at $p = 0.5$.

Figure 7 describes the transformation of the coefficient of directed light scattering $\beta_1(\theta)$ as the contribution of t–fraction increases at other constant parameters of the microstructure $r_{min} = 0.4$ μm, $\nu = 2$, and $r_m = 15$ μm.

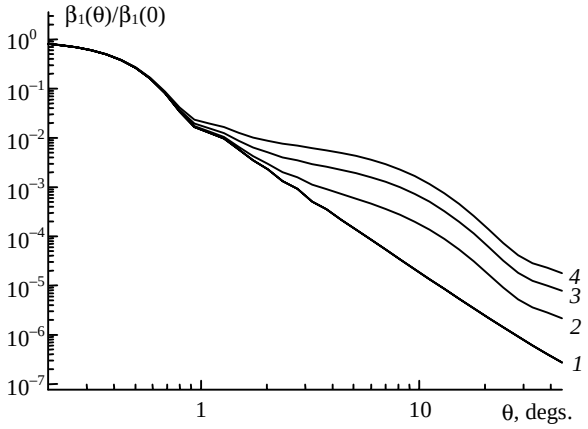

Fig. 7. Angular dependence of the directed light scattering coefficient $\beta_1(\theta)/\beta_1(0)$ for the polydisperse suspension of particles in water with the microstructure parameters $\nu = 2$, $r_{min} = 0.4$ μm, and $r_m = 15$ μm at $p = 0$ (*1*), 0.2 (*2*), 0.5 (*3*), and 0.7 (*4*).

The effect of the tilt of the distribution $s_t(r)$ on the behavior of the directed light scattering coefficient $\beta_1(\theta)$ at variations of the parameter ν and $r_{min} = 0.4$ μm is shown in Fig. 8. In this case, as in Fig. 5, the fractions of contributions of both fractions to the scattering coefficient was equal ($p = 0.5$). Curve *5* describes the scattering phase function by only the particles of t–fraction.

One can relate the conclusions drawn in discussing Fig. 5 relative to division of the small-angle range into two zones with prevalent effect of different fractions of the suspension in each of them to the results shown in Figs. 7 and 8.

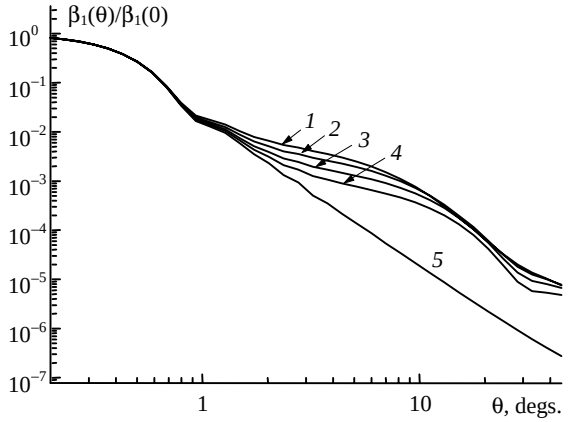

Fig. 8. Angular dependence of the directed light scattering coefficient $\beta_1(\theta)/\beta_1(0)$ for the polydisperse suspension of particles in water with the parameters of the microstructure $r_{min} = 0.4$ μm and $r_m = 15$ μm at $p = 0.5$ and $\nu = 1$ (*1*), 2 (*2*), 3 (*3*) and 4 (*4*).

For conclusion, let us briefly consider how the changes in the scattering phase functions observed at the variations of the microstructure of the suspension affect the behavior of their Hankel transformations. Examples of the Hankel transformation $\tilde{x}_1(\rho)$ are shown in Figs. 9 and 10 as a function of the argument $\rho = p/k$ for the scattering phase functions shown in Figs. 5 and 6. As in Fig. 5, curve *1* in Fig. 9 corresponds to the situation when the particles of both fractions have been totally taken into account in calculations of $\tilde{x}_1(\rho)$. The contrary case corresponding to the account of particles of b–fractions only in the small-angle scattering pattern is shown by curve *5*. Curves *2–4* describe the transformation of $\tilde{x}_1(\rho)$ as the contributions of particles of the size less than 0.4 (curve *2*), 0.6 (*3*), and 0.8 μm (*4*) were removed from consideration.

The function $\tilde{x}_1(\rho)$ is monotonically decreasing. Its peculiarity is that the value $\tilde{x}_1(\rho)$ at each value $\rho = p/k$ depends only on the microstructure of the particles the radius of which is $r > \rho/2$. As a result, two characteristic scales are selected in the curves under consideration: the range of small values ρ less than 4 μm that is characterized by steep slope of the curves and in which the joint manifestations of both fractions is observed, and the range with a more slant decrease of $\tilde{x}_1(\rho)$ at $\rho > 4$ μm formed exclusively by the particles of the b–fraction. Position of the ordinate on the dependences $\tilde{x}_1(\rho)$ in the vicinity of the change of the slope characterizes the ratio of the contributions from t– and b–fractions to the small-angle scattering coefficient σ_1.

The series expansion of $\tilde{x}_1(\rho)$ over the components corresponding to t- (curve *1*) and b- (*2*) fractions of particles for curve *3* (see Fig. 9) is shown in Fig. 10. It is seen from Fig. 10 that curve *2* in the range of small ρ

values changes insignificantly, and the change of $\tilde{x}_1(\rho)$ occurs due to b–fraction.

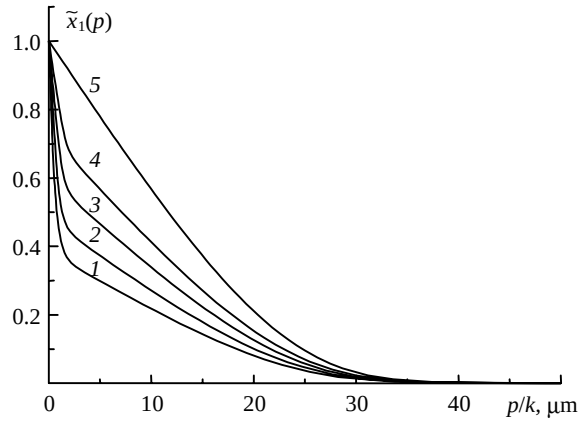

Fig. 9. The Hankel transformation $\tilde{x}_1(\rho)$ of the small-angle scattering phase function for the polydisperse suspension of particles in water with the microstructure parameters: $\nu = 2$, $r_m = 15$ μm, $p = 0.5$ and $r_{min} = 0.2$ (*1*), 0.4 (*2*), 0.6 (*3*), 0.8 (*4*), and 2.0 μm (*5*).

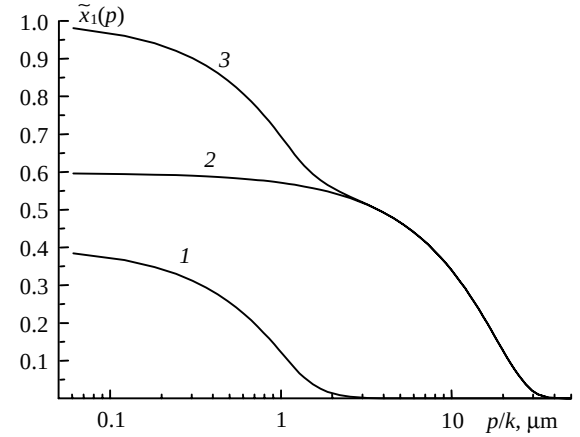

Fig. 10. Components of the Hankel transformation $\tilde{x}_1(\rho)$ for the particles of mineral fraction (*1*) with the parameters $\nu = 2$, $r_{min} = 0.6$ μm and biogenic fractions (*2*) with the modal radius $r_m = 15$ μm and their sum (*3*) at $p = 0.5$.

Conclusion

The variability of the small-angle characteristics of scattering by disperse suspensions in seawater at variations of the parameters of their microstructure is studied by means of numerical modeling. The Hankel transformation, small-angle asymmetry factor and the effective size of scatterers were considered in addition to the scattering phase function. The list of characteristics chosen was dictated first of all by the requirements to the *a priori* data for solving the inverse problems of lidar sounding of seawater taking into account multiple scattering.

It has been supposed, when choosing the microstructure parameters, that the suspension was formed from two fractions of particles: fine fraction of terrigenic origin and coarse fraction of biogenic origin. The calculated results are an evidence of the necessity to take into account the contribution of terrigenic fraction, without which the small-angle pattern of scattering essentially changes.

The lower-size boundary of particles of terrigenic fraction is established, for which the small-angle asymmetry factor is practically invariant at variations of the ratio of fraction in a wide range. The small-angle asymmetry factor is also weakly sensitive to the change of the modal radius of particles of biogenic fraction. The areas have been isolated and their size estimated for the scattering phase functions and their Hankel transformations, in which the noted fractions of the suspension dominate in formation of these characteristics. The results presented are useful for interpretation of the data of lidar measurements.

References

1. L.S. Dolin and V.A. Savel'ev, Izv. Akad. Nauk SSSR, Fiz. Atmos. Okeana **7**, No. 5, 505–510 (1971).
2. B.V. Ermakov and Yu.A. Il'inskii, Izv. Vyssh. Uchebn. Zaved. SSSR, Ser. Radiofizika **12**, No. 5, 694–701 (1969).
3. L.S. Dolin, Izv. Vyssh. Uchebn. Zaved. SSSR, Ser. Radiofizika **7**, No. 2, 380–382 (1964).
4. L.B. Scotts, J. Opt. Soc. Am. **67**, No. 6, 815–819 (1977).
5. V.I. Burenkov, O.V. Kopelevich, and K.S. Shifrin, Izv. Akad. Nauk SSSR, Ser. Fiz. Atmos. Okeana **11**, No. 8, 828–835 (1975).
6. V.E. Zuev, V.V. Belov, and V.V. Veretennikov, *Theory of Systems in Optics of Disperse Media* (Spektr, Tomsk, 1997), 402 pp.
7. V.V. Veretennikov, Proc. SPIE **3983**, 260–270 (1999).
8. M. Born and E. Wolf, *Principles of Optics* (Pergamon Press, New York, 1964).
9. H. C. van de Hulst, *Light Scattering by Small Particles* (Willey, New York, 1957).
10. A.S. Monin, ed., *Ocean Optics*. Vol. 1, *Physical Optics of the Ocean* (Nauka, Moscow, 1983), 372 pp.